Electrostatic repulsion causes anticooperative DNA binding between tumor suppressor ETS transcription factors and JUN–FOS at composite DNA sites

Received for publication, May 9, 2018, and in revised form, October 2, 2018 Published, Papers in Press, October 12, 2018, DOI 10.1074/jbc.RA118.003352

Bethany J. Madison[‡§1], **Kathleen A. Clark**[‡§1], **Niraja Bhachech**[‡§], **Peter C. Hollenhorst**[¶], **Barbara J. Graves**[‡§‖2], **and Simon L. Currie**[‡§3]

From the [‡]*Department of Oncological Sciences and* [§]*Huntsman Cancer Institute, University of Utah School of Medicine, Salt Lake City, Utah 84112, the* [¶]*Medical Sciences program, Indiana University School of Medicine, Bloomington, Indiana 47405, and the* [‖]*Howard Hughes Medical Institute, Chevy Chase, Maryland 20815*

Edited by Joel M. Gottesfeld

Many different transcription factors (TFs) regulate gene expression in a combinatorial fashion, often by binding in close proximity to each other on composite *cis*-regulatory DNA elements. Here, we investigated how ETS TFs bind with the AP1 TFs JUN–FOS at composite DNA-binding sites. DNA-binding ability with JUN–FOS correlated with the phenotype of ETS proteins in prostate cancer. We found that the oncogenic ETS-related gene (ERG) and ETS variant (ETV) 1/4/5 subfamilies co-occupy ETS–AP1 sites with JUN–FOS *in vitro*, whereas JUN–FOS robustly inhibited DNA binding by the tumor suppressors ETS homologous factor (EHF) and SAM pointed domain–containing ETS TF (SPDEF). EHF bound ETS–AP1 DNA with tighter affinity than ERG in the absence of JUN–FOS, possibly enabling EHF to compete with ERG and JUN–FOS for binding to ETS–AP1 sites. Genome-wide mapping of EHF- and ERG-binding sites in prostate epithelial cells revealed that EHF is preferentially excluded from closely spaced ETS–AP1 DNA sequences. Structural modeling and mutational analyses indicated that adjacent positively charged surfaces from EHF and JUN–FOS use electrostatic repulsion to disfavor simultaneous DNA binding. Conservation of positive residues on the JUN–FOS interface identified E74-like ETS TF 1 (ELF1) as an additional ETS TF exhibiting anticooperative DNA binding with JUN–FOS, and we found that ELF1 is frequently down-regulated in prostate cancer. In summary, divergent electrostatic features of ETS TFs at their JUN–FOS interface enable distinct binding events at ETS–AP1 DNA sites, which may drive specific targeting of ETS TFs to facilitate distinct transcriptional programs.

This work was supported in part by National Institutes of Health Grants R01GM38663 (to B. J. G.) and R01CA204121 (to P. C. H.). The authors declare that they have no conflicts of interest with the contents of this article. The content is solely the responsibility of the authors and does not necessarily represent the official views of the National Institutes of Health.
This article contains Figs. S1–S11, Tables S1–S9 and supporting Refs. 1–14.
RNA sequences generated in this study have been deposited in the NCBI Gene Expression Omnibus (GEO) with accession numbers GSE114241, GSM3138379, GSM3138380, and GSM3138381.

[1] Both authors contributed equally to this work.
[2] Supported by the Huntsman Cancer Institute/Huntsman Cancer Foundation and the Howard Hughes Medical Institute. To whom correspondence should be addressed: Tel.: 301-215-8718; Fax: 301-215-8828; E-mail: barbara.graves@hci.utah.edu.
[3] Present address: Dept. of Biophysics, University of Texas Southwestern Medical Center, Dallas, TX 75390.

Sequence-specific TFs[4] bind to *cis*-regulatory elements in enhancers and promoters to regulate gene expression. Composite DNA sequences consisting of multiple TF-binding sites enable precise and combinatorial control of gene transcription by integrating multiple inputs into a single transcriptional output (1, 2). Multiple TFs can bind to a composite DNA sequence in a cooperative (tighter affinity for DNA), non-cooperative (same affinity for DNA), or anticooperative (reduced affinity for DNA) manner. In many cases, TFs modulate the binding of each other at composite binding sites through protein–protein interactions (3–6) and/or through DNA-mediated effects (7–10). Although combinatorial regulation of gene transcription occurs frequently (4), the molecular basis of interplay between most TF pairings at composite sites is poorly understood.

Closely-apposed sites for the binding of ETS and AP1 TFs play an important role in regulating cellular migration. These composite sites are found in the enhancers and promoters of genes such as the urokinase plasminogen activator (*PLAU*), the uridine phosphorylase (*UPP*), and the matrix metalloproteases (*MMP1*, *MMP9*, etc.) (11–14). Overexpression of "oncogenic" ETS factors from the ERG and ETV1/4/5 subfamilies occurs frequently in prostate cancers (15, 16) and leads to the hyperactivation of ETS–AP1-regulated genes, ultimately resulting in enhanced cellular migration (11). Correspondingly, these oncogenic ETS factors bind to composite ETS–AP1 sites with JUN–FOS *in vitro* (17). Conversely, other ETS factors such as EHF and SPDEF function as tumor suppressors in prostate cancer (18–20) and repress the transcription of ETS–AP1-regulated genes (11, 13). A simple hypothesis is that the tumor suppressor class of factors competes with oncogenic ones for binding to ETS–AP1 composite sites. However, no direct evidence for this hypothesis is available.

Here, we investigate the difference between oncogenic and tumor suppressor ETS factors in binding to ETS–AP1 sites with JUN–FOS. Oncogenic proteins bound to composite sites with

[4] The abbreviations used are: TF, transcription factor; ERG, ETS-related gene; ETV, ETS variant; EHF, ETS homologous factor; SPDEF, SAM pointed domain–containing ETS TF; PMSF, phenylmethanesulfonyl fluoride; FDR, false discovery rate; βME, 2-mercaptoethanol; qPCR, quantitative PCR; EMSA, electrophoretic mobility shift assay.

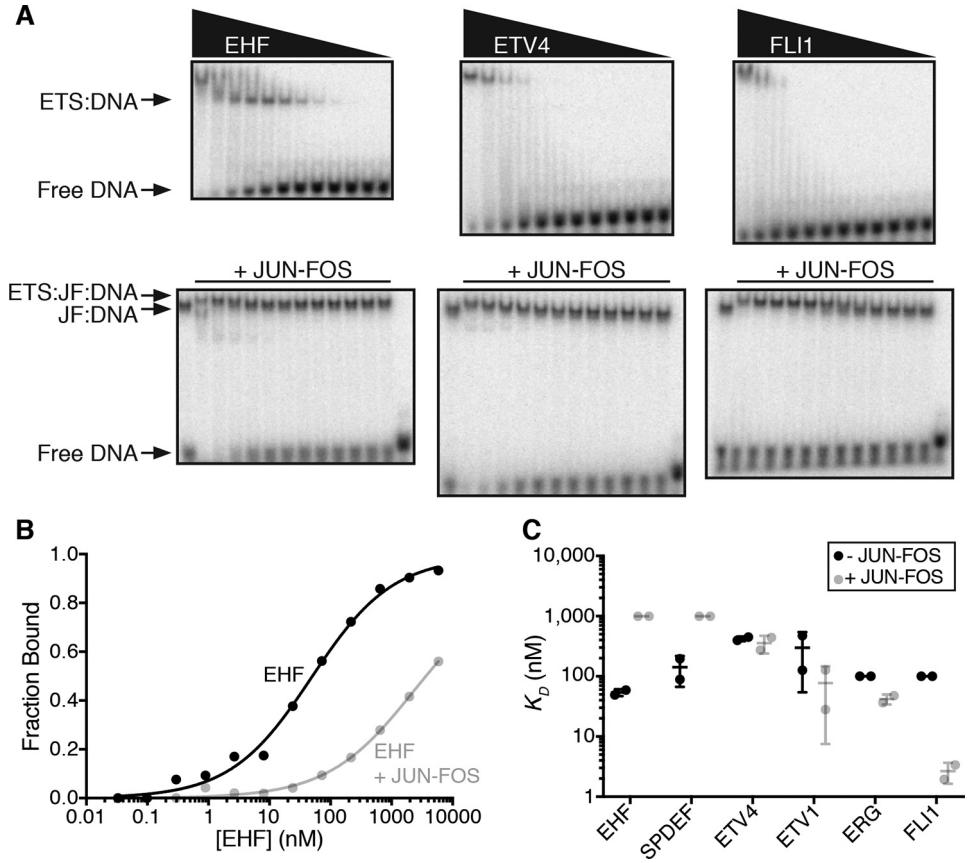

Figure 1. JUN–FOS differentially influences the DNA binding of ETS factors to AP1–ETS composite sites. *A,* representative phosphorimages of EMSAs for EHF (*left*), ETV4 (*middle*), and FLI1 (*right*) binding to the *UPP* promoter DNA duplex. ETS titrations were performed with DNA alone (*top*), and with JUN–FOS bound to the DNA (*bottom*). JUN–FOS EMSAs contain two control lanes; the *1st lane* with indicated ETS factor and DNA and the *last lane* with DNA only. The *higher band* for EHF corresponds to two EHF molecules bound to the DNA duplex, as observed previously for similar ETS factors (17). *B,* binding isotherms for EHF binding to *UPP* DNA in the absence (*black*) and presence (*gray*) of JUN–FOS. *C,* K_D values for ETS factors binding to *UPP* DNA without (*black*) and with (*gray*) JUN–FOS. *Lines* indicate the mean and standard deviation from two experiments (*filled circles*). Minimal K_D values of 1000 nM were estimated for EHF and SPDEF binding to *UPP* promoter DNA with JUN–FOS as binding isotherms for these low-affinity interactions do not approach saturation. Similarly, minimal K_D values of 100 nM were estimated for ERG and FLI1 binding to *UPP* promoter DNA. See Fig. S1 and Table S1 for quantification of K_D values and fold differences.

JUN–FOS in either a cooperative (ERG and FLI1) or noncooperative manner (ETV1 and ETV4). In contrast, the tumor suppressors EHF, SPDEF, and ELF1 displayed a robust anticooperative binding to DNA with JUN–FOS. In the absence of JUN–FOS, EHF bound to ETS–AP1 sequences with higher affinity than ERG suggesting that the inability of EHF to co-occupy DNA with JUN–FOS is not due to intrinsic DNA-binding differences. Genome-wide mapping of EHF and ERG DNA-binding sites in a prostate epithelial cell line provided support for anticooperative DNA binding between EHF and JUN–FOS at closely spaced ETS–AP1 composite sites. Structural modeling suggested that simultaneous DNA binding would result in electrostatic repulsion between positive surfaces of EHF and JUN–FOS. In contrast, the corresponding surface on ERG is polar and negative, complementing the positive interface of JUN–FOS. In support of this model, mutation of lysine residues in EHF enabled binding to DNA with JUN–FOS. Our results indicate that electrostatic properties regulate the ability of ETS factors to bind to composite ETS–AP1 DNA sequences with JUN–FOS and implicate the divergence of these properties in the phenotypically diverse roles of ETS factors in prostate cancer.

Results

JUN–FOS differentially impacts ETS factor binding to composite ETS–AP1 sites

Oncogenic ETS factors, such as those from the ERG and ETV1/4/5 subfamilies, enhance transcription at ETS–AP1-regulated genes; conversely, ETS tumor suppressors, such as EHF and SPDEF, repress transcription from ETS–AP1-regulated genes (11, 13, 18, 20). We hypothesized that differences in binding to DNA with JUN–FOS may be one reason for differential regulation by ETS factors. To test this hypothesis, we expressed and purified full-length recombinant proteins for AP1 factors JUN and FOS and for the ETS factors ETV1, ETV4, ERG, FLI1, EHF, and SPDEF. We measured the equilibrium dissociation constant (K_D) for ETS proteins binding to an ETS–AP1 composite DNA sequence from the *UPP* promoter using electrophoretic mobility shift assays (EMSAs) in the presence and absence of JUN–FOS (Fig. 1, Fig. S1, and Table S1). JUN–FOS enhanced the DNA-binding affinity of FLI1 (greater than 40-fold), had minimal effects on the affinity of ERG (greater than 2-fold), ETV1 (4 ± 3-fold (mean ± S.D.)), and ETV4 (1.2 ± 0.3-fold), and strongly reduced the DNA-binding affinity of

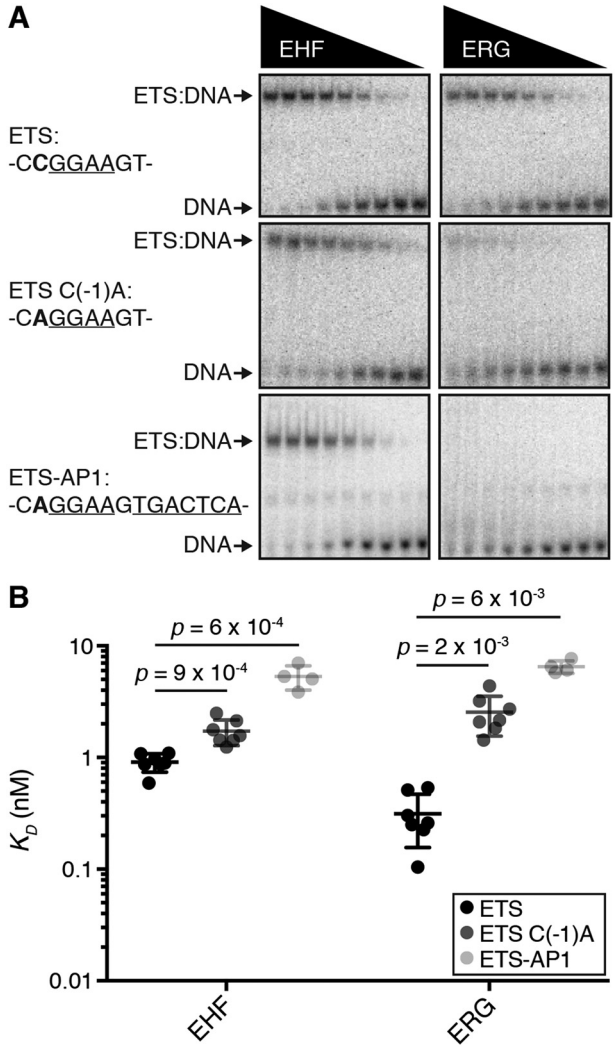

Figure 2. Single-nucleotide change flanking core ETS-binding sequence differentially affects the DNA binding of ETS factors. *A,* representative EMSAs for EHF (*left*) and ERG (*right*) with three different DNA duplexes. DNA sequences are listed on the *left* and consist of a consensus ETS DNA sequence (*ETS*), a single nucleotide change from the ETS consensus sequence that is present in ETS–AP1 composite motifs (*ETS C(-1)A*), and an ETS–AP1 composite DNA sequence (*ETS–AP1*). ETS and AP1 DNA-binding sites are *underlined,* and the single nucleotide change is in *bold*. *B,* K_D values for EHF and ERG with different DNA sequences. See Table S2 and Fig. S2 for quantification of EMSAs.

EHF (greater than 20-fold) and SPDEF (greater than 10-fold). These findings suggest that different subgroups of ETS factors display cooperative, noncooperative, or anticooperative binding with JUN–FOS to an ETS–AP1 composite DNA sequence.

We also observed that ETS factors in the absence of JUN–FOS have distinct binding affinities for the ETS–AP1 sequence in the *UPP* promoter; EHF bound to this promoter with roughly 10-fold higher affinity than ERG, FLI1, ETV1, and ETV4 (Fig. 1*C*). We next tested EHF and ERG with a series of DNA sequences to further investigate this difference in binding to DNA. We found that ERG binds to a consensus high-affinity ETS-binding sequence "SC1" (21, 22) with 3-fold higher affinity than EHF (3 ± 1-fold; Fig. 2, Fig. S2, and Table S2). ERG and EHF had comparable affinities for another ETS–AP1 DNA-binding sequence from the enhancer of *COPS8*, indicating that sequence differences in this enhancer preferentially disfavor ERG. The proximal 5′-nucleotide outside of the core ETS motif is a cytosine (CGGAA) in the consensus ETS sequence, but it is an adenosine (AGGAA) in many ETS–AP1-binding sites, including those at the *UPP* promoter and *COPS8* enhancer (11, 17). The nucleotide at this position has previously been shown to selectively affect the DNA binding of different ETS factors (22, 23). To test whether this single nucleotide difference is important in selectively weakening ERG binding relative to EHF binding, we changed this nucleotide from cytosine to adenosine in the context of the high-affinity ETS sequence SC1 (Fig. 2) (21). This single change largely recapitulated the difference in binding affinities observed for the ETS–AP1 sequence, *i.e.* ERG bound to this DNA with 8-fold weaker affinity (8 ± 5-fold), and the disruption of EHF binding was more subtle (1.9 ± 0.6-fold; Fig. 2 and Fig. S2). Therefore, in the absence of JUN–FOS, EHF has a higher affinity for ETS–AP1 DNA sequences compared with oncogenic ETS factors. The tighter affinity of EHF may allow it to compete with ERG for ETS–AP1 DNA sequences despite binding anticooperatively with JUN–FOS.

ERG and EHF display differential preference for composite ETS–AP1 sites in vivo

To explore the biological significance of the cooperativity and anticooperativity displayed by ERG and EHF with JUN–FOS, respectively, we examined binding site preferences for these two proteins *in vivo*. Specifically, full-length ERG- or EHF-coding sequence was tagged with FLAG and expressed retrovirally in RWPE1 cells, a normal prostate epithelial cell line, and then FLAG-ChIPs were performed to determine chromatin occupancy genome-wide. ERG and EHF proteins were expressed at similar levels as judged by Western blot analysis (Fig. S3*A*). Cluster analysis of the ChIP-seq data sets for ERG–FLAG and EHF–FLAG revealed four distinct groups: 1) regions with both high ERG and EHF occupancy; 2) regions with high EHF occupancy and low ERG occupancy; 3) regions with high ERG occupancy and low EHF occupancy; and 4) regions with low but significant occupancy for both proteins (Fig. 3*A*). Thus, ERG and EHF exhibit both redundant and unique genomic targets in RWPE1 cells.

Because of the high number of occupied regions, we limited further analysis to the top 1000 enriched regions for both proteins. Both ChIP datasets were enriched for DNA motifs matching the ETS-binding consensus sequence (Fig. 3*B*), with slight differences in nucleotide preference surrounding the core GGA. The previously described composite "ETS–AP1 half-site" (CAGGAA(A/G)TGA) (11) was specifically enriched in the ERG dataset. Full AP1 sites (TGANTCA) were also over-represented in both datasets (Fig. 3*B*). The composite element displaying tight spacing between ETS and AP1 motifs, which we examined by EMSAs, was more enriched in the ERG dataset as compared with the EHF dataset (Fig. 3*C*). Conversely, ETS–AP1 composite sites with more distant spacing were similarly represented in both ERG and EHF datasets. We conclude that anticooperative DNA binding between EHF and JUN–FOS is limited to ETS–AP1 composite sites with tight spacing.

To interrogate our genome-wide findings by quantifying differences in occupancy between ERG and EHF, we performed

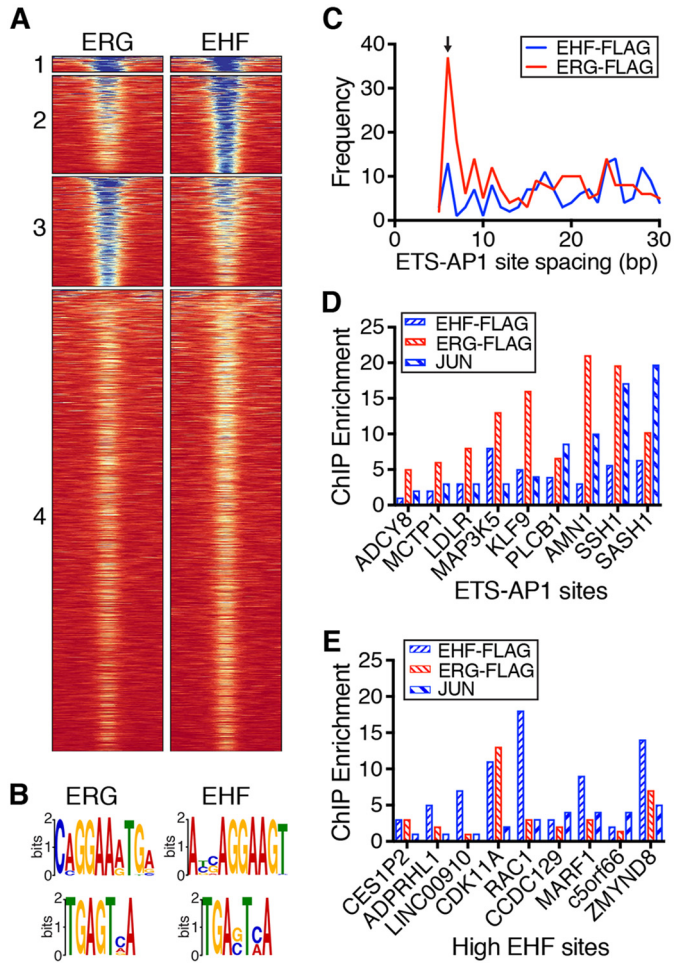

Figure 3. Preferential binding of ERG to ETS–AP1 sites *in vivo*. *A,* heat map of reads for ERG–FLAG and EHF–FLAG ChIP data; *numbers* at *left* indicate clusters referred to in the text. Analysis of ChIPseq data using MACS2 returned 34,746 enriched regions for ERG–FLAG and 44,977 for EHF–FLAG. *B*, ETS (*top*) and AP1 (*bottom*) DNA-binding sequences are enriched in ERG- and EHF-binding sites as determined by MEME (56). *C,* spacing between ETS and AP1 sites in top 1000 EHF–FLAG and ERG–FLAG ChIP peaks; spacing is defined as nucleotide distance between core ETS (GGAA) and AP1 (TGANTCA) DNA recognition motifs (11). *Arrow* indicates the ETS–AP1 spacing that was used in EMSAs. *D,* qPCR quantification of EHF–FLAG, ERG–FLAG, and JUN enrichment at putative regulatory elements for genes shown; regions selected based on match to ETS–AP1 sites with +6 spacing as indicated by the *arrow* in *C*. Two to three independent biological replicates provided similar patterns but different maximum levels of enrichment. A representative experiment is shown. *E,* qPCR quantification of EHF–FLAG, ERG–FLAG, and JUN enrichment at regions predicted to have high EHF occupancy based on ChIPseq data. ChIP enrichment for *D* and *E* is defined as the qPCR signal for that site divided by the qPCR signal for a neutral region, the 3′ UTR of *BCLxL1*.

direct ChIP–qPCR on randomly selected regions from the ERG–FLAG ChIP data that had an ETS–AP1 site with tight spacing. JUN occupancy was also confirmed in these direct ChIPs. Occupancy was defined by ChIP enrichment, the ratio of the PCR signal from a test region compared with a control region. At seven of the eight ETS–AP1 sites assayed, ChIP enrichment was at least 2-fold and up to 7-fold higher for ERG than EHF (Fig. 3*D* and Fig. S3*B*); thus, ERG–FLAG occupancy at regions with composite ETS–AP1 sites was higher than EHF–FLAG occupancy, as suggested by the motif analysis in the genome-wide analysis. JUN occupancy was similar at most ETS–AP1 sites in RWPE1 cells expressing either ERG or EHF suggesting that the presence of JUN–FOS may be deterring EHF binding (Fig. S3*C*). Additionally, JUN was depleted from two ETS–AP1 sites at enhancers for *SASH1* and *PLCB1* in EHF-expressing cells indicating that EHF may prevent JUN–FOS from binding to select ETS–AP1 sites. To verify that lower EHF occupancy at ETS–AP1 sites did not reflect a detection problem of EHF *versus* ERG in cells, we assayed regions that were specifically enriched for EHF in the cluster analysis. At specific EHF-enriched sites, EHF occupancy was equal or greater than ERG (Fig. 3*D*). JUN occupancy was also lower at these regions compared with regions with preferential ERG binding. Collectively, these data suggest that ERG and EHF have distinct DNA-binding profiles in prostate cancer cells, including the relative depletion of EHF at closely spaced ETS–AP1 composite sites.

Positive residues N-terminal of, and within, the ETS domain of EHF mediate anticooperative binding to DNA with JUN–FOS

To characterize the anticooperative binding to DNA with JUN–FOS, which we had observed for both EHF and SPDEF, we chose EHF for mapping the minimal regions of EHF and JUN–FOS that were sufficient for anticooperative DNA binding. The DNA-binding domains of JUN ($JUN^{\Delta N250;\ \Delta C319}$) and FOS ($FOS^{\Delta N131;\ \Delta C203}$) were sufficient for antagonizing the DNA binding of full-length EHF (Fig. S4). Residues 193–300 of EHF ($EHF^{\Delta N193}$), which includes the ETS domain and 16 residues N-terminal of the ETS domain, retained the full anticooperative binding behavior of the full-length protein, a greater than 20-fold decrease due to the presence of JUN–FOS (Fig. 4). Removal of the flanking N-terminal residues ($EHF^{\Delta N203}$) improved binding to DNA in the presence of JUN–FOS, although $EHF^{\Delta N203}$ still retained 4-fold (4 ± 3-fold) anticooperative behavior. Therefore, the minimal regions required for anticooperative DNA binding for JUN and FOS are the DNA-binding domains, although in the case of EHF both the ETS domain and a proximal N-terminal region are needed.

We next generated a structural model to interrogate the differential binding between ETS factors with JUN–FOS at composite ETS–AP1 sites using previously characterized DNA-bound structures of JUN–FOS (24) and ETS factors ERG (25) and ELF3 (26), which is a close homolog of EHF. To model the ternary complex, we aligned the DNA sequences to mimic a common composite site with the ETS site just upstream of the AP1 site (GAGGAAGTGACTCA) (11). This modeling demonstrated no significant steric overlap for the ETS domain of EHF or ERG binding with JUN–FOS to the composite motif. However, the regions on the ETS domains of EHF and ERG in closest proximity to JUN–FOS have contrasting charge properties. For EHF, the N terminus of the ETS domain, the loop between α-helices H2 and H3, and the C terminus of H3 are all positively charged, whereas the analogous regions in ERG are neutral or negatively charged (Fig. 5, *A* and *B*, and Fig. S5). The regions of JUN and FOS proximal to ETS factors are positively charged. Therefore, our modeling suggests that the positively-charged interfaces of EHF and JUN–FOS would cause electrostatic repulsion, disfavoring simultaneous binding to composite DNA sequences. In contrast, the lack of positive charges in the ERG interface presents a more favorable interaction surface for JUN–FOS allowing for concurrent binding with JUN–FOS to composite DNA sequences.

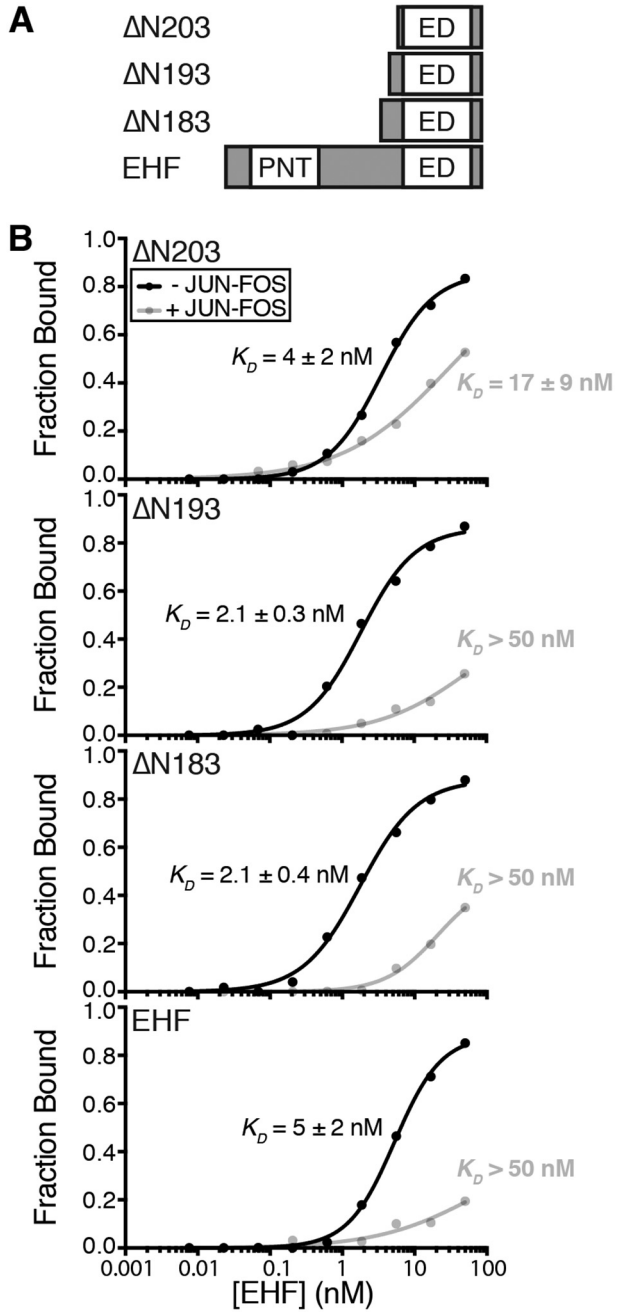

Figure 4. Sequences N-terminal to the ETS domain and within the ETS domain of EHF are important for anticooperative binding with JUN–FOS to composite ETS–AP1 sites. *A*, schematic of EHF truncation series. ETS DNA-binding domain (*ED*) and Pointed domain (*PNT*) are labeled. *B*, representative binding isotherms for EHF and N-terminal truncations binding to an ETS–AP1 sequence without (*black*) and with (*gray*) JUN–FOS. K_D values (mean ± S.D.) from four experiments are listed. Minimal K_D values for EHF, EHF$^{\Delta N183}$, and EHF$^{\Delta N193}$ binding to DNA with JUN–FOS were estimated as these binding isotherms do not approach saturation. See Fig. S4 for representative EMSA images and Table S5 for quantification.

Next, we tested the functional importance of positive residues within EHF for anticooperative binding with JUN–FOS to composite sites. Four positively-charged regions of EHF were mutated: the N-terminal region preceding the ETS domain (K196E, K200E, and K201E); the loop between β-strand S2 and α-helix H2 (K241E, S242P, and A244E); the loop between α-helices H2 and H3 (K251E and K252Q); and the C-terminal end of α-helix H3 (K272E) (Fig. 5*C*). These regions were selected based on being more positively charged in ETS factors that displayed anticooperative binding with JUN–FOS (Figs. S5 and S6). The EHF residues within the ETS domain were mutated to corresponding residues in ETS factors that bind with JUN–FOS to composite sites, and the lysine residues in N-terminal region preceding the ETS domain were mutated to glutamate residues, as there is no meaningful sequence alignment for this region between different subfamilies of ETS factors (Fig. S6). Mutant proteins were tested for binding to DNA alone and with JUN–FOS. Importantly, these mutations did not significantly change the binding of EHF to DNA in the absence of JUN–FOS (Fig. S7). However, mutating the region N-terminal to the ETS domain completely ablated anticooperative DNA binding with JUN–FOS (Fig. 5*D* and Fig. S7). Mutation of H3, and to a lesser extent the H2–H3 loop, showed lower impact. As a control, mutation of the S2–H2 loop, which is on the opposite side of the ETS domain from JUN–FOS in this ETS–AP1 composite motif arrangement, did not alter EHF binding with JUN–FOS. Therefore, positive residues in EHF that form the JUN–FOS interface are important for the anticooperative binding of EHF and JUN–FOS to ETS–AP1 DNA sequences.

ELF1 also exhibits anticooperative DNA binding with JUN–FOS

To further explore the role of basic residues in anticooperative binding, we tested DNA binding of other ETS factors with JUN–FOS. We selected ERF, GABPA, ELF1, and ELK4 for further analysis as these factors represent ETS factor subfamilies that have not been examined previously (17) or in this study (Fig. S8). Like EHF, ELF1 has positive residues in all three of the positions that contribute to anticooperative binding with JUN–FOS (Fig. 6*A* and Fig. S6). In contrast, ERF, GABPA, and ELK4 lack positive residues in at least one of these important regions (Fig. S6). JUN–FOS antagonized ELF1 DNA binding and slightly enhanced ELK4, ERF, and GABPA binding to DNA (Fig. 6, *B* and *C*, and Fig. S9). These additional data allowed us to predict the effect of JUN–FOS on the remaining untested ETS factors based on sequence homology (Figs. S6 and S8). Comparing the charge of ETS domains and flanking regions demonstrates that ETS factors that anticooperatively bind to DNA with JUN–FOS tend to be more positively charged than other ETS factors (Fig. S8*B*). These data suggest that ELF1 binds anticooperatively with JUN–FOS due to a similar electrostatic repulsion mechanism as observed for EHF.

Discussion

Here we report the variable binding of ETS transcription factors with JUN–FOS to composite DNA sequences. DNA binding of the tumor suppressors EHF and SPDEF is antagonized by JUN–FOS, in contrast to oncogenic factors from the ERG and ETV1/4/5 subfamilies. We propose that this difference in binding to DNA with JUN–FOS contributes to the opposing impact on the transcription of ETS–AP1-regulated genes by oncogenic and tumor suppressor ETS factors (Fig. 7*A*) (11, 13).

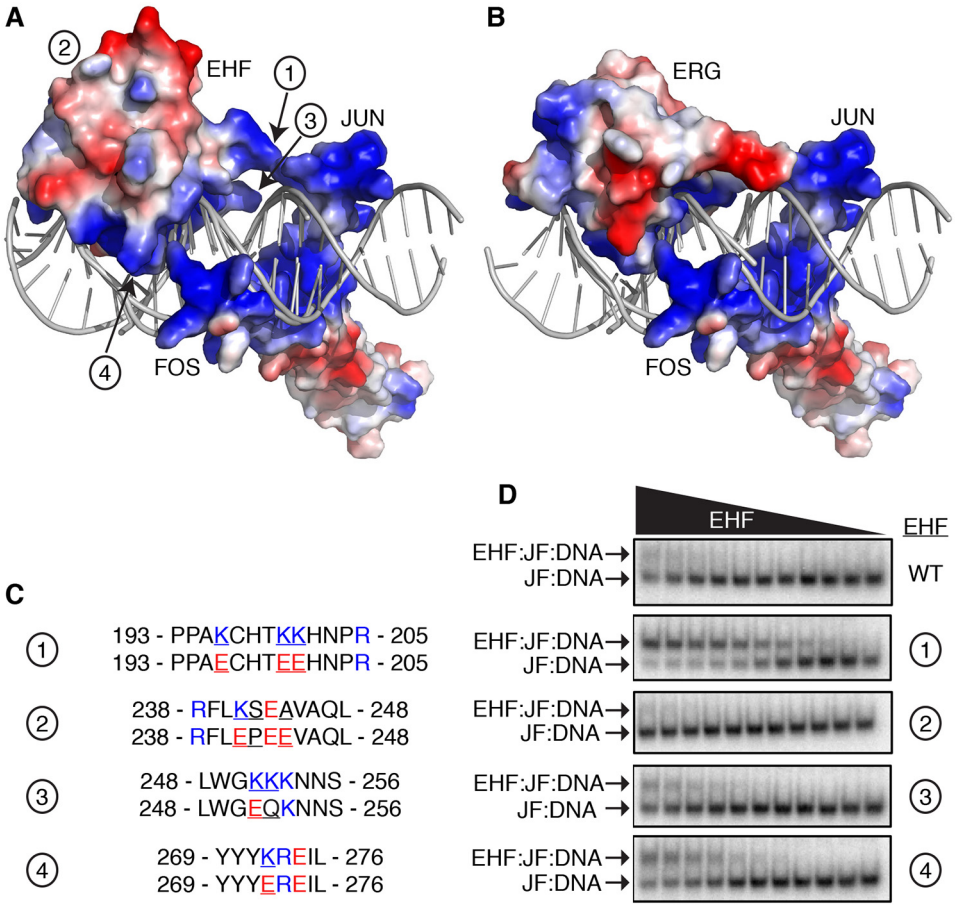

Figure 5. Positively-charged residues near the JUN–FOS interface are important for anticooperative binding of EHF and JUN–FOS. *A* and *B*, structural model of EHF (*A*) and ERG (*B*) binding to an ETS–AP1 composite DNA sequence with JUN–FOS. EHF, ERG, and JUN–FOS are shown in surface mode and colored according to electrostatic potential (*red,* negative; *blue,* positive). Regions of EHF that were subsequently mutated are labeled *1–4* in *A*. Note that EHF residues 193–204 are not present in this modeled structure. *C*, listing of EHF residues that were mutated. *Circled numbers 1–4* correspond to the regions labeled in *A*. The *top* and *bottom sequences* indicate the native and mutated residues, respectively. Residues are colored according to charge, as in *A*. *D*, portions of EMSAs showing EHF wildtype (*WT*) and mutants bound in the presence of JUN–FOS on an ETS–AP1 site. EHF was serially diluted in 2-fold increments. Bands corresponding to JUN–FOS bound to DNA (*JF:DNA*) as well as EHF and JUN–FOS bound to DNA (*EHF:JF:DNA*) are labeled. See Fig. S7 and Table S6 for further quantification of EMSAs.

Model for anticooperative DNA binding between EHF and JUN–FOS

Residues flanking and within the ETS domain of EHF contribute to anticooperative DNA binding with JUN–FOS, as revealed by a truncation series. In particular, the region including multiple lysine residues N-terminal to the ETS domain is the single strongest contributor to this effect. Structural modeling indicated that the N terminus of the ETS domain as well as the loop between α-helices H2 and H3 and the C-terminal end of H3 are all positioned at the JUN–FOS interface when both factors are bound to DNA. These three regions of ETS factors, although separate in primary sequence, converge in the tertiary structure to form a tripartite interface. In EHF, all of these regions are positively charged and are positioned near the positively-charged regions of the DNA-binding domains of JUN and FOS. Therefore, we suggest that electrostatic repulsion between basic EHF and JUN–FOS surfaces inhibits simultaneous DNA binding in this orientation. In contrast, the collective JUN–FOS interface on ERG is composed of negative and polar residues, making ERG more suitable for simultaneous DNA binding with JUN–FOS. Mutation of EHF to eliminate basic residues along this interface at any of the three regions abrogated anticooperative binding with JUN–FOS. Eliminating basic residues from the region N-terminal to the ETS domain again demonstrated the largest effect, matching the truncation series data. However, mutation of the H2–H3 loop or the C terminus of H3 also significantly improved the DNA binding of EHF with JUN–FOS, indicating that positive residues at all three sites contribute to the full anticooperative effect. Interestingly, further examination of additional ETS factors demonstrated that ELF1, which is positively charged at all three analogous regions, exhibited anticooperative DNA binding with JUN–FOS. In contrast, ERF and ELK4, which lack positively-charged residues in at least one of these regions, do not exhibit anticooperative DNA binding. Finally, introduction of the positive residues from EHF into any single site of the tripartite interface on ERG (*i.e.* N-terminal, H2–H3 loop, or C terminus of H3) failed to transfer any level of anticooperative binding with JUN–FOS into ERG (data not shown). Therefore, we propose that anticooperative binding to DNA with JUN–FOS requires all three stretches of positive residues on EHF that cumulatively form a basic interface with JUN–FOS (Fig. 7*B* and Fig. S10).

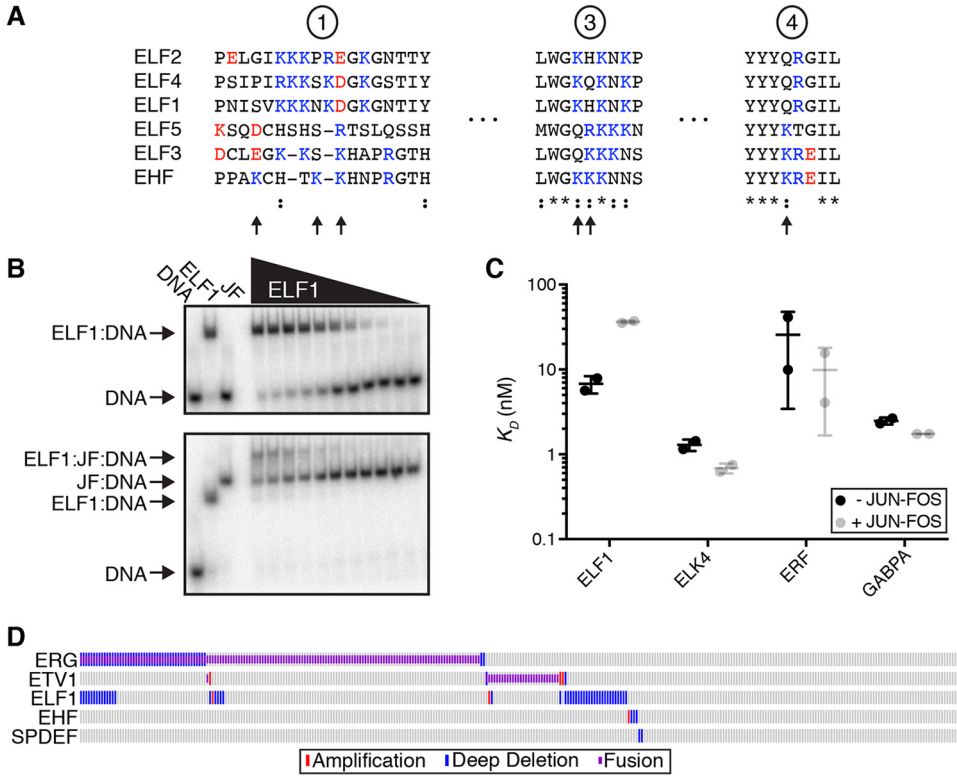

Figure 6. ELF1 also exhibits anticooperative DNA binding with JUN–FOS. *A*, sequence alignment of EHF and ELF1/2/4 subfamilies for regions important for anticooperative DNA binding with JUN–FOS. *Numbers above sequences* and *arrows below sequences* refer to EHF regions and residues mutated in Fig. 5. See Fig. S6 for complete sequence alignments. *B*, representative EMSAs for ELF1 alone (*top*) and with JUN–FOS (*bottom*). The *first three lanes* correspond to DNA only, ELF1:DNA, and JUN–FOS:DNA (*bottom gel* only) controls. *C*, comparison of K_D values for ELF1, ELK4, ERF, and GABPA alone (*black*) and with JUN–FOS (*gray*). *Filled circles* indicate an individual experiment, and *lines* indicate the mean and S.D. See Table S7 for K_D values and Fig. S9 for representative EMSAs of ELK4, ERF, and GABPA. *D*, example of an oncoprint curated from cBioPortal showing mutational frequencies of the ETS factors ERG, ETV1, ELF1, EHF, and SPDEF (http://www.cbioportal.org) (31, 32). (Please note that the JBC is not responsible for the long-term archiving and maintenance of this site or any other third party hosted site.) This example is from a 2015 TCGA prostate cancer study (34). ERG and ETV1 are frequently overexpressed through gene fusions, and EHF and SPDEF are rarely present in deep deletions, as characterized previously (15, 16, 19, 20). Interestingly, ELF1 is also frequently involved in deep deletions suggesting that it may be a tumor suppressor in prostate cancer. See Fig. S11 for additional studies with frequent ELF1 gene deletions in prostate cancer patients.

Despite close proximity to the DNA interaction surface, elimination of basic residues from the JUN–FOS interface of EHF did not significantly impact DNA binding in the absence of JUN–FOS. We interpret this to indicate that DNA binding alone and anticooperative DNA binding with JUN–FOS are fundamentally different and separable properties. Correspondingly, the arginine and tyrosine residues along the core DNA-recognition surface of α-helix H3 are highly conserved across ETS factors (Figs. S6 and S10) (22, 27). Nevertheless, our data do not exclude the possibility that alteration to DNA structure upon JUN–FOS binding may disfavor EHF binding. Further structural characterization of cooperative FLI1 and JUN–FOS DNA binding, as well as molecular simulations of anticooperative EHF and JUN–FOS DNA binding, would help to determine whether through-DNA effects contribute to the disparate binding behavior that we have observed for ETS and JUN–FOS factors binding to composite DNA sites.

Anticooperative ETS factors, such as EHF, ELF1, SPDEF, and SPI1, bind with slightly stronger affinities to ETS–AP1 DNA sequences in the absence of JUN–FOS compared with cooperative ETS factors. These data suggest that when present in excess, anticooperative ETS factors will compete with oncogenic ETS factors and JUN–FOS for binding to ETS–AP1 sites. In principle, this competition would reduce the level of transcription from ETS–AP1-regulated genes by reducing the occupancy of oncogenic ETS factors and/or JUN–FOS (Fig. 7*A*). This hypothesis is supported by previously reported data indicating that anticooperative ETS factors are highly expressed in normal prostate cells and dampen the transcription of genes involved in cellular migration that are regulated by ETS–AP1 sites (11, 13, 17, 28). Therefore, we propose that anticooperative DNA binding with JUN–FOS is one mechanism for tumor suppressor ETS factors to repress the transcription of ETS–AP1-regulated genes.

Distinct mechanisms of transcriptional repression among ETS factors

We originally examined the anticooperative ETS factors EHF and SPDEF based on their reported tumor suppressor roles in prostate cancer (18–20). Thus, we hypothesized that other positively charged ETS factors that bind to DNA in an anticooperative manner with JUN–FOS might also behave as tumor suppressors in prostate cancer. Publicly available data support this hypothesis, as protein levels of ELF and SPI subfamily members ELF1, ELF2, ELF4, and SPIB are often down-regulated in prostate cancer samples (Fig. S11*A*) (29, 30). Furthermore, at the genomic level, *ELF1* in particular is affected by deep gene deletions in up to 20% of prostate cancer samples

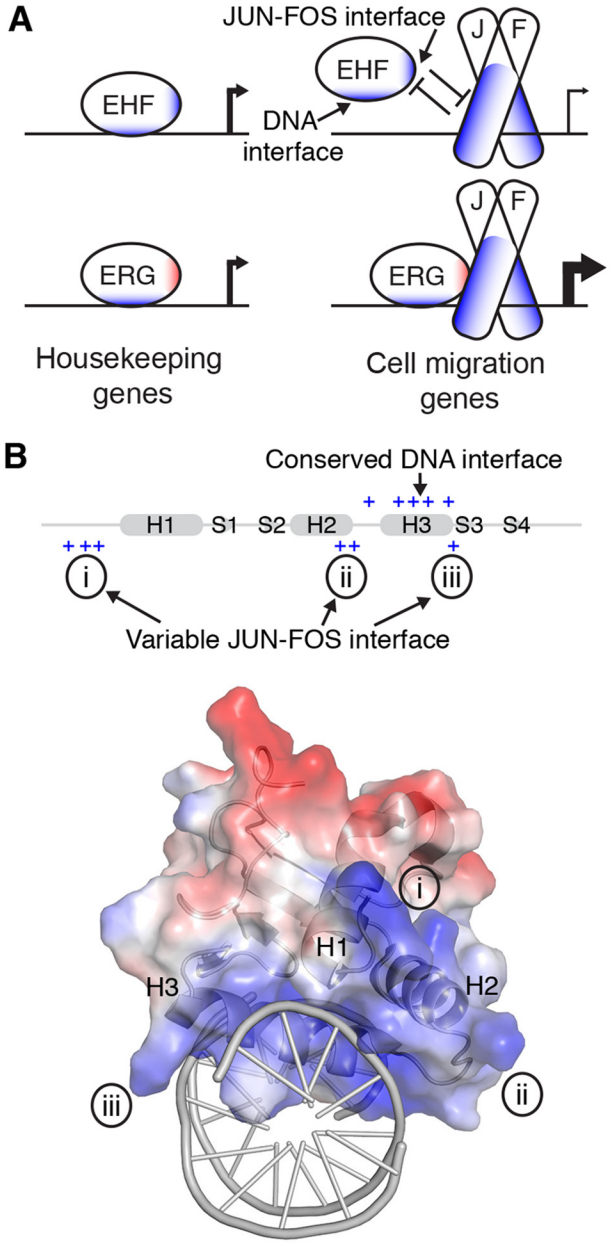

Figure 7. Model for differential regulation of ETS–AP1 sites by ETS factors. *A, left,* EHF and ERG have DNA-binding surfaces similar to all ETS factors and therefore bind to ETS DNA sequences with relatively similar affinities. *Right,* distinct JUN–FOS interface of EHF and ERG allows ERG to bind to ETS–AP1 sequences with JUN–FOS but prevents EHF from binding to ETS–AP1 sequences with JUN–FOS. This difference in binding affinities is consistent with the repression and activation of ETS–AP1-regulated genes by EHF and ERG, respectively (11, 13). *B*, three positive regions of EHF form the JUN–FOS interface. *Top,* ETS domain of EHF is depicted in cartoon format; *cylinders* and *arrows* indicate α-helices and β-strands, respectively, and are named according to previous nomenclature (27). Positive residues in α-helix H3 are at the primary DNA interface and are highly conserved among human ETS factors (Figs. S6 and S8). In contrast, positive residues N-terminal to the ETS domain (*i*), in the H2–H3 loop (*ii*), and C terminus of α-helix H3 (*iii*) form the JUN–FOS interface and are only found in a subset of human ETS factors. *Bottom*, these three regions of EHF, which are separated in primary sequence, converge to form a broad positively-charged interface for JUN–FOS. See Fig. S10 for the JUN–FOS interfaces of SPDEF, ELF1, and ERG.

from different prostate cancer studies (Fig. 6*D* and Fig. S11*B*) (31–38). Our functional DNA-binding data suggest that ELF1 behaves similarly to EHF and SPDEF. Therefore, given the high frequency of gene deletions in prostate cancer patients, we suggest that the potential role of ELF1 as a tumor suppressor should be further investigated.

A recent report implicated the ETS factor ERF as a novel tumor suppressor in prostate cancer and suggested that ERF represses transcription from ERG and androgen receptor target genes by competing with ERG for binding to ETS DNA sequences (39). Our analysis of an ERF truncation (residues 1–126) indicates that ERF cooperatively binds to ETS–AP1 DNA sequences with JUN–FOS, unlike the other ETS tumor suppressors that we tested. Although we cannot rule out that full-length ERF may behave differently, several lines of evidence support that ERF transcriptional repression occurs through a distinct mechanism as compared with EHF, ELF1, and SPDEF. The repressor domain of ERF is distal from the ETS DNA-binding domain, greater than 350 residues away in primary sequence, and is fully transferable to a heterologous protein (40). In contrast, the positive residues of EHF that facilitate anticooperative DNA binding with JUN–FOS flank or are within the DNA-binding domain and are not easily transferable to other proteins, such as ERG. Furthermore, ERF acts as a transcriptional repressor in all contexts tested thus far (40), whereas EHF represses or activates genes in a context-dependent manner (13, 41). These data suggest that ERF-mediated transcriptional repression occurs at a level other than DNA binding, such as through the recruitment of transcriptional corepressors. In contrast, our results suggest that anticooperative binding to DNA with JUN–FOS is a distinct mechanism of transcriptional repression that may contribute to the tumor suppressor phenotypes of the ETS factors EHF and SPDEF in prostate cancer (18–20, 35, 42).

Diversification of interaction surfaces enables functional regulation

Individual ETS transcription factors display diverse developmental and disease-related phenotypes (27, 43), yet they possess ETS domains with remarkably similar DNA-binding preferences (22). How might this apparent contradiction be explained? One route for specificity involves the use of composite DNA sequences for combinatorial regulation. For example, composite ETS–RUNX sites are found in T-cell activation genes, and ETS1 specifically regulates these genes through cooperatively binding to DNA with RUNX1 (6, 10, 23, 44). FLI1 binds cooperatively to DNA with JUN–FOS, although the molecular basis for this cooperativity remains unclear (17). Here, we demonstrate that a subset of ETS factors, including SPDEF, EHF, and ELF1, bind to DNA in an anticooperative manner with JUN–FOS. This anticooperativity depends on positively charged residues from multiple regions of the protein that together form the JUN–FOS interface. The JUN–FOS-interacting surface is distinct from the conserved DNA-binding surface, enabling precise control on modulating transcriptional activity at genes regulated by ETS–AP1 composite sites without impacting other genes that are regulated by ETS sites. An analogous electrostatic repulsion mechanism has recently been described for the selective recognition of appropriate substrates by tyrosine kinases involved in T-cell signaling (45, 46). Therefore, electrostatic selection may be a general mechanism for

fine-tuning molecular interactions that contribute to the phenotypic diversity of large gene families.

Materials and methods

Expression plasmids

Open reading frames corresponding to full-length or truncated JUN, EHF, ELF1, ELK4, ERF, ERG, ETV1, ETV4, FLI1, FOS, GABPA, and SPDEF were cloned into the bacterial expression vector pET28 as described previously (47, 48). Point mutations were introduced into the EHF ΔN193 plasmid using the QuikChange site-directed mutagenesis protocol (Stratagene).

Expression and purification of proteins

ETS proteins were expressed in *Escherichia coli* (λDE3) cells. Full-length EHF and truncated ETS proteins (see Table S8 for protein sequences) were efficiently expressed into the soluble fraction. One-liter cultures of Luria broth (LB) were grown at 37 °C to an A_{600} of ~0.7. The cultures were then induced with 0.5 mM isopropyl β-D-thiogalactopyranoside for approximately 3 h at 30 °C. Cultures were centrifuged at 12,000 × *g* for 10 min at 4 °C. Cells were resuspended with 25 ml of buffer (per liter of culture) containing 25 mM Tris, pH 7.9, 1 M NaCl, 0.1 mM EDTA, 2 mM 2-mercaptoethanol (βME), and 1 mM phenylmethanesulfonyl fluoride (PMSF), flash-frozen in liquid nitrogen, and stored at −80 °C. Cells were lysed by sonication and centrifuged at 125,000 × *g* for 30 min at 4 °C. The supernatant containing the soluble fraction was loaded onto a Ni^{2+} affinity column (GE Biosciences) and eluted over a 5–500 mM imidazole gradient. Fractions containing purified protein were pooled and dialyzed overnight at 4 °C into a buffer containing 25 mM Tris, pH 7.9, 10% glycerol (v/v), 1 mM EDTA, 50 mM KCl, and 1 mM dithiothreitol (DTT). After centrifugation at 125,000 × *g* for 30 min at 4 °C, the soluble fraction was loaded onto an SP-Sepharose cation-exchange column or Q-Sepharose anion-exchange column (GE Biosciences), depending on the pI value of the individual protein, and then eluted by a linear gradient from 50 mM to 1 M NaCl. Fractions containing purified protein were pooled and further purified by size-exclusion chromatography on a Superdex 75 column run with a buffer containing 25 mM Tris, pH 7.9, 10% glycerol, 1 mM EDTA, and 300 mM KCl. Fractions containing purified protein were pooled and concentrated by 30-, 10-, or 3-kDa molecular mass cutoff Centricon devices (Sartorius). Concentrated proteins were snap-frozen with liquid nitrogen and stored at −80 °C in single-use aliquots for subsequent EMSA studies.

Full-length ERG, FLI1, ETV1, ETV4, and SPDEF were predominantly expressed into inclusion bodies (see Table S8 for protein sequences). Protein expression was induced and then cells were centrifuged and stored as described above, with the exception of ETV4, which was induced by autoinduction as described previously (48, 49). After the initial sonication, the samples were centrifuged at 31,000 × *g* for 15 min at 4 °C, and then the soluble fraction was discarded. This procedure was performed a total of three times to wash the inclusion bodies in 25 mM Tris, pH 7.9, 1 M NaCl, 0.1 mM EDTA, 5 mM imidazole, 2 mM βME, and 1 mM PMSF. The final insoluble pellet was resuspended in a buffer containing 25 mM Tris, pH 7.9, 1 M NaCl, 0.1 mM EDTA, 5 mM imidazole, 2 mM βME, 1 mM PMSF, and 6 M urea using sonication. After rotation for ~1 h at 4 °C, the sample was centrifuged at 125,000 × *g* for 30 min at 4 °C. The soluble fraction was loaded onto a Ni^{2+} affinity column and refolded on-column by switching to the same buffer lacking urea. After elution with a 5–500 mM imidazole gradient, the remaining purification steps (ion-exchange and size-exclusion chromatography) were performed, as described above.

Full-length JUN and FOS proteins were expressed and purified as described previously (50, 51). Briefly, JUN and FOS expressed into the insoluble fraction and were expressed and purified as above, with the following exceptions. FOS was expressed in Rosetta 2 cells (Novagen) for supplementation of rare Arg tRNAs. Inclusion bodies were purified and solubilized as described above, and then JUN and FOS were combined for JUN–FOS heterodimers, diluted to 200 ng/μl (total protein), and then dialyzed for at least 3 h each against the following three buffers (in sequential order): 1) 25 mM Tris, pH 6.7, 0.1 mM EDTA, 10% glycerol, 5 mM βME, 1 M NaCl, 1 M urea; 2) same as 1 but without urea; and 3) same as 2 but with NaCl reduced to 100 mM. Refolded samples were then purified by Ni^{2+} affinity and size-exclusion chromatography, as described above.

Truncated $JUN^{\Delta N250;\,\Delta C319}$ and $FOS^{\Delta N131;\,\Delta C203}$ proteins expressed into the insoluble fraction and were solubilized as described above. $JUN^{\Delta N250;\,\Delta C319}$ and $FOS^{\Delta N131;\,\Delta C203}$ were then individually loaded onto a Ni^{2+} affinity column, refolded on-column, and eluted, as described above. $JUN^{\Delta N250;\,\Delta C319}$ and $FOS^{\Delta N131;\,\Delta C203}$ were then combined to form heterodimers and further purified by size-exclusion chromatography, as described above.

EMSA

DNA-binding assays of ETS factors utilized duplexed oligonucleotides corresponding to the promoter or enhancer regions of the genes *UPP1* and *COPS8*, respectively, and a consensus high-affinity ETS-binding site SC1 (Selected Clone 1) (11, 17, 21). The DNA sequences for these oligonucleotides are listed in Table S8. Each pair of oligonucleotides, at 2 μM as measured by absorbance at 260 nm on a NanoDrop 1000 (ThermoFisher Scientific), was labeled with [γ-^{32}P]ATP using T4 polynucleotide kinase at 37 °C for 30 min. After purification over a Bio-Spin 6 chromatography column (Bio-Rad), the oligonucleotides were incubated at 100 °C for 5 min and then cooled to room temperature over ~2 h. The DNA concentration for EMSAs was diluted to 5×10^{-11} M and held constant. JUN–FOS was titrated against each DNA sequence to determine near-saturating amounts, where bound DNA was ~80% of total DNA. For the *UPP* promoter, full-length JUN–FOS was included at 1 μM, whereas the truncated JUN–FOS was included at 100 nM for the *COPS8* enhancer. In a series of equilibrium binding reactions, ETS factor concentrations were varied from the micromolar to the sub-nanomolar range to determine the equilibrium dissociation constant (K_D) for ETS factors on DNA or on JUN–FOS–DNA complexes. Protein concentrations were determined after thawing each aliquot of protein using the Protein Assay Dye Reagent (Bio-Rad). The binding reactions were incubated for 3 h at 4 °C in a buffer containing 25

mM Tris, pH 7.9, 0.1 mM EDTA, 60 mM KCl, 6 mM $MgCl_2$, 200 μg/ml bovine serum albumin, 10 mM DTT, 100 ng/μl poly-(dI-dC), and 10% (v/v) glycerol. The fractions of bound *versus* nonbound species were resolved on a 4 or 6% (w/v) native polyacrylamide gel run at 4 °C for experiments with full-length or truncated JUN–FOS, respectively. The ^{32}P-labeled DNA was quantified on dried gels by phosphorimaging on a Typhoon Trio Variable Mode Imager (Amersham Biosciences). Equilibrium dissociation constants (K_D) were determined by nonlinear least-squares fitting of the total ETS protein concentration $[P]_t$ *versus* the fraction of DNA bound ($[PD]/[D]_t$) to the equation $[PD]/[D]_t = B_{max}\cdot[P]_y^h/(K_D^h + [P]_t^h)$ with Prism (version 7; GraphPad Software), with B_{max} indicating maximum specific binding and h indicating the Hill slope. To determine ETS factor K_D values in the presence of JUN–FOS, the PD in this formula was represented by [PPD], the signal from doubly occupied DNA. Because of the low concentration of total DNA, $[D]_t$, in all reactions, the total protein concentration is a valid approximation of the free, unbound protein concentration. Individual experiments were fit using the equation above, and K_D values are reported as mean ± S.D. for the indicated number of replicate experiments. Statistical *t* tests were calculated with Graph Pad Prism (Version 7.0b) for experiments with at least three replicates. Consistent standard deviation was not assumed, and the two-stage step-up false discovery rate (FDR) approach of Benjamini *et al.* (52) was used with a desired FDR of 1%.

Cell culture and viral expression

RWPE1 cells were obtained from American Type Culture Collection and cultured accordingly. Full-length ERG and EHF cDNAs with an added C-terminal 3xFLAG tag were cloned into a modified pLHCX retroviral expression vector (Clontech) with the cytomegalovirus promoter replaced by the HNRPA2B1 promoter. Expression and infection of retrovirus were performed following standard protocols. Whole-cell extracts from cells expressing empty constructs, ERG–FLAG, or EHF–FLAG were run on SDS-polyacrylamide gels and blotted to nitrocellulose membranes following standard procedures. Antibodies used for immunodetection were FLAG (M2, Sigma) and β-actin (C4, ThermoFisher Scientific).

ChIP and ChIPseq analysis

ChIPs were performed as described previously (53), with the following modifications. Cross-linked chromatin was sheared with a Branson sonifier, and magnetic beads were washed with buffer containing 500 mM LiCl. Antibodies used for ChIP were as follows: anti-FLAG (M2, Sigma) and anti-c-JUN (E254, Abcam). ChIPseq libraries were prepared using the NEBNext® ChIP-Seq Library Prep Master Mix Set for Illumina (New England Biolabs, E6240) and run on a Hiseq2000 sequencer. Sequence reads were aligned with Novoalign to human genome HG19, and enriched regions (peaks) were determined using the MACS2 analysis package (54). Heat maps of enriched regions for ERG–FLAG and EHF–FLAG ChIPseq were generated with DeepTools (55) using a bed file corresponding to coordinates from the combined ChIPseq bed files, and bigwig files generated from the individual ChIPseq datasets. Data were aligned using the center point of this shared peak bed file.

Over-represented DNA sequences present in the ERG–FLAG and EHF–FLAG enriched regions were determined using the MEME-ChIP program (http://meme-suite.org)[5] (56, 57) using default settings except for following parameters for MEME: 1) any number of repetitions for site distribution; and 2) maximum site width of 13. ETS–AP1 sites spacings were determined using Regulatory Sequence Analysis Tools (58) searching the top 1000 ChIPseq peaks for the ERG–FLAG and EHF–FLAG datasets.

Primer-BLAST (59) was used to generate primer sets for amplification of enriched regions; primer sequences and the coordinates of interrogated regions are provided in Table S9. qPCR of ChIP DNA was performed using Roche FastStart Essential DNA Green Master and run on a Lightcycler 96 (Roche Applied Science). Serially diluted input was used to create a standard curve for absolute quantitation of amplified regions from ChIP DNA. PCRs for each sample and primer pair were run as triplicates and signal averaged over the three values. Data are displayed in graphical form as a ratio of the signal of the target region over the signal of a negative control genomic region. An input sample was also subject to the same qPCRs graphed to confirm validity of negative control region. For all primer pairs, the input enrichment value was approximately 1.

Structural modeling

Structural models for ETS and JUN–FOS factors binding to a composite DNA sequence were constructed with PyMOL (Version 1.7.0.5) and the following Protein Data Bank entries: ERG, 4IRI (25); JUN–FOS, 1FOS (24); ELF3, 3JTG (26). A homology model of EHF was generated from the closely related ELF3 by manual mutation of distinct residues. ETS and JUN–FOS molecules were oriented by aligning DNA nucleotides to create an ETS–AP1 composite sequence, such as those found in the *UPP* promoter and the *COPS8* enhancer (Table S8). The overlapping DNA from the ETS and JUN–FOS structures does not perfectly align, suggesting that DNA distortions may occur in the ternary complex. We cannot rule out that through DNA effects may also contribute to the anticooperative DNA binding exhibited by EHF and JUN–FOS.

Protein Atlas and cBioPortal data curation

Protein levels for ETS factors in normal prostate and prostate cancer samples were curated from The Protein Atlas (https://www.proteinatlas.org)[5] (29, 30). Data are reported for ELF1, ELF2, ELF4, and SPIB; these ETS factors, or close homologs (Figs. S6, S8, and S9), have been shown to bind to ETS–AP1 DNA in an anticooperative manner with JUN–FOS here or as described previously (17). These four factors are expressed at a "medium" level in normal prostate cells so "low" or "no detection" in prostate cancer cells represents down-regulation at the protein level. TCGA data were curated from cBioPortal (http://www.cbioportal.org)[5] (31, 32). Several prostate cancer genomic studies revealed recurrent gene deletions of ELF1 in up to 20%

[5] Please note that the JBC is not responsible for the long-term archiving and maintenance of this site or any other third party hosted site.

of patient samples (33–38). An example from one study is represented in Fig. 6*D*, and all studies with substantial ELF1 deletions are listed in Fig. S11*B*.

Author contributions—B. J. M., K. A. C., N. B., P. H., and S. L. C. data curation; B. J. M., K. A. C., N. B., P. H., B. J. G., and S. L. C. formal analysis; B. J. M., K. A. C., N. B., P. H., and S. L. C. investigation; B. J. M., K. A. C., N. B., P. H., B. J. G., and S. L. C. methodology; B. J. M., K. A. C., N. B., P. H., B. J. G., and S. L. C. writing-review and editing; K. A. C., P. H., B. J. G., and S. L. C. conceptualization; K. A. C., P. H., B. J. G., and S. L. C. supervision; K. A. C., P. H., B. J. G., and S. L. C. writing-original draft; N. B. validation; P. H. resources; B. J. G. funding acquisition; B. J. G. project administration; S. L. C. visualization.

Acknowledgments—We thank Mahesh Chandrasekharan, Jedediah Doane, and members of the Graves lab for helpful discussion. Shared resources at the University of Utah were supported by the National Institutes of Health Grant P30CA042014 to the Huntsman Cancer Institute.

References

1. Lee, T. I., and Young, R. A. (2000) Transcription of eukaryotic protein-coding genes. *Annu. Rev. Genet.* **34,** 77–137 CrossRef Medline
2. Panne, D. (2008) The enhanceosome. *Curr. Opin. Struct. Biol.* **18,** 236–242 CrossRef Medline
3. Garvie, C. W., Pufall, M. A., Graves, B. J., and Wolberger, C. (2002) Structural analysis of the autoinhibition of Ets-1 and its role in protein partnerships. *J. Biol. Chem.* **277,** 45529–45536 CrossRef Medline
4. Jolma, A., Yin, Y., Nitta, K. R., Dave, K., Popov, A., Taipale, M., Enge, M., Kivioja, T., Morgunova, E., and Taipale, J. (2015) DNA-dependent formation of transcription factor pairs alters their binding specificity. *Nature* **527,** 384–388 CrossRef Medline
5. LaRonde-LeBlanc, N. A., and Wolberger, C. (2003) Structure of HoxA9 and Pbx1 bound to DNA: Hox hexapeptide and DNA recognition anterior to posterior. *Genes Dev.* **17,** 2060–2072 CrossRef Medline
6. Shrivastava, T., Mino, K., Babayeva, N. D., Baranovskaya, O. I., Rizzino, A., and Tahirov, T. H. (2014) Structural basis of Ets1 activation by Runx1. *Leukemia* **28,** 2040–2048 CrossRef Medline
7. Joshi, R., Passner, J. M., Rohs, R., Jain, R., Sosinsky, A., Crickmore, M. A., Jacob, V., Aggarwal, A. K., Honig, B., and Mann, R. S. (2007) Functional specificity of a Hox protein mediated by the recognition of minor groove structure. *Cell* **131,** 530–543 CrossRef Medline
8. Kim, S., Broströmer, E., Xing, D., Jin, J., Chong, S., Ge, H., Wang, S., Gu, C., Yang, L., Gao, Y. Q., Su, X. D., Sun, Y., and Xie, X. S. (2013) Probing allostery through DNA. *Science* **339,** 816–819 CrossRef Medline
9. Panne, D., Maniatis, T., and Harrison, S. C. (2007) An atomic model of the interferon-β enhanceosome. *Cell* **129,** 1111–1123 CrossRef Medline
10. Shiina, M., Hamada, K., Inoue-Bungo, T., Shimamura, M., Uchiyama, A., Baba, S., Sato, K., Yamamoto, M., and Ogata, K. (2015) A novel allosteric mechanism on protein-DNA interactions underlying the phosphorylation-dependent regulation of Ets1 target gene expressions. *J. Mol. Biol.* **427,** 1655–1669 CrossRef Medline
11. Hollenhorst, P. C., Ferris, M. W., Hull, M. A., Chae, H., Kim, S., and Graves, B. J. (2011) Oncogenic ETS proteins mimic activated RAS/MAPK signaling in prostate cells. *Genes Dev.* **25,** 2147–2157 CrossRef Medline
12. Bosc, D. G., Goueli, B. S., and Janknecht, R. (2001) HER2/Neu-mediated activation of the ETS transcription factor ER81 and its target gene MMP-1. *Oncogene* **20,** 6215–6224 CrossRef Medline
13. Tugores, A., Le, J., Sorokina, I., Snijders, A. J., Duyao, M., Reddy, P. S., Carlee, L., Ronshaugen, M., Mushegian, A., Watanaskul, T., Chu, S., Buckler, A., Emtage, S., and McCormick, M. K. (2001) The epithelium-specific ETS protein EHF/ESE-3 is a context-dependent transcriptional repressor downstream of MAPK signaling cascades. *J. Biol. Chem.* **276,** 20397–20406 CrossRef Medline
14. Plotnik, J. P., Budka, J. A., Ferris, M. W., and Hollenhorst, P. C. (2014) ETS1 is a genome-wide effector of RAS/ERK signaling in epithelial cells. *Nucleic Acids Res.* **42,** 11928–11940 CrossRef Medline
15. Tomlins, S. A., Rhodes, D. R., Perner, S., Dhanasekaran, S. M., Mehra, R., Sun, X. W., Varambally, S., Cao, X., Tchinda, J., Kuefer, R., Lee, C., Montie, J. E., Shah, R. B., Pienta, K. J., Rubin, M. A., and Chinnaiyan, A. M. (2005) Recurrent fusion of TMPRSS2 and ETS transcription factor genes in prostate cancer. *Science* **310,** 644–648 CrossRef Medline
16. Tomlins, S. A., Mehra, R., Rhodes, D. R., Smith, L. R., Roulston, D., Helgeson, B. E., Cao, X., Wei, J. T., Rubin, M. A., Shah, R. B., and Chinnaiyan, A. M. (2006) TMPRSS2:ETV4 gene fusions define a third molecular subtype of prostate cancer. *Cancer Res.* **66,** 3396–3400 CrossRef Medline
17. Kim, S., Denny, C. T., and Wisdom, R. (2006) Cooperative DNA binding with AP-1 proteins is required for transformation by EWS-Ets fusion proteins. *Mol. Cell. Biol.* **26,** 2467–2478 CrossRef Medline
18. Albino, D., Longoni, N., Curti, L., Mello-Grand, M., Pinton, S., Civenni, G., Thalmann, G., D'Ambrosio, G., Sarti, M., Sessa, F., Chiorino, G., Catapano, C. V., and Carbone, G. M. (2012) ESE3/EHF controls epithelial cell differentiation and its loss leads to prostate tumors with mesenchymal and stem-like features. *Cancer Res.* **72,** 2889–2900 CrossRef Medline
19. Cangemi, R., Mensah, A., Albertini, V., Jain, A., Mello-Grand, M., Chiorino, G., Catapano, C. V., and Carbone, G. M. (2008) Reduced expression and tumor suppressor function of the ETS transcription factor ESE-3 in prostate cancer. *Oncogene* **27,** 2877–2885 CrossRef Medline
20. Cheng, X. H., Black, M., Ustiyan, V., Le, T., Fulford, L., Sridharan, A., Medvedovic, M., Kalinichenko, V. V., Whitsett, J. A., and Kalin, T. V. (2014) SPDEF inhibits prostate carcinogenesis by disrupting a positive feedback loop in regulation of the Foxm1 oncogene. *PLoS Genet.* **10,** e1004656 CrossRef Medline
21. Nye, J. A., Petersen, J. M., Gunther, C. V., Jonsen, M. D., and Graves, B. J. (1992) Interaction of murine ets-1 with GGA-binding sites establishes the ETS domain as a new DNA-binding motif. *Genes Dev.* **6,** 975–990 CrossRef Medline
22. Wei, G. H., Badis, G., Berger, M. F., Kivioja, T., Palin, K., Enge, M., Bonke, M., Jolma, A., Varjosalo, M., Gehrke, A. R., Yan, J., Talukder, S., Turunen, M., Taipale, M., Stunnenberg, H. G., *et al.*. (2010) Genome-wide analysis of ETS-family DNA-binding *in vitro* and *in vivo*. *EMBO J.* **29,** 2147–2160 CrossRef Medline
23. Hollenhorst, P. C., Chandler, K. J., Poulsen, R. L., Johnson, W. E., Speck, N. A., and Graves, B. J. (2009) DNA specificity determinants associate with distinct transcription factor functions. *PLoS Genet.* **5,** e1000778 CrossRef Medline
24. Glover, J. N., and Harrison, S. C. (1995) Crystal structure of the heterodimeric bZIP transcription factor c-Fos-c-Jun bound to DNA. *Nature* **373,** 257–261 CrossRef Medline
25. Regan, M. C., Horanyi, P. S., Pryor, E. E., Jr., Sarver, J. L., Cafiso, D. S., and Bushweller, J. H. (2013) Structural and dynamic studies of the transcription factor ERG reveal DNA binding is allosterically autoinhibited. *Proc. Natl. Acad. Sci. U.S.A.* **110,** 13374–13379 CrossRef Medline
26. Agarkar, V. B., Babayeva, N. D., Wilder, P. J., Rizzino, A., and Tahirov, T. H. (2010) Crystal structure of mouse Elf3 C-terminal DNA-binding domain in complex with type II TGF-β receptor promoter DNA. *J. Mol. Biol.* **397,** 278–289 CrossRef Medline
27. Hollenhorst, P. C., McIntosh, L. P., and Graves, B. J. (2011) Genomic and biochemical insights into the specificity of ETS transcription factors. *Annu. Rev. Biochem.* **80,** 437–471 CrossRef Medline
28. Hollenhorst, P. C., Jones, D. A., and Graves, B. J. (2004) Expression profiles frame the promoter specificity dilemma of the ETS family of transcription factors. *Nucleic Acids Res.* **32,** 5693–5702 CrossRef Medline
29. Uhlen, M., Zhang, C., Lee, S., Sjostedt, E., Fagerberg, L., Bidkhori, G., Benfeitas, R., Arif, M., Liu, Z., Edfors, F., Sanli, K., von Feilitzen, K., Oksvold, P., Lundberg, E., Hober, S., *et al.* (2017) A pathology atlas of the human cancer transcriptome. *Science* **357,** pii: eaan2507 CrossRef Medline
30. Uhlén, M., Fagerberg, L., Hallström, B. M., Lindskog, C., Oksvold, P., Mardinoglu, A., Sivertsson, Å., Kampf, C., Sjöstedt, E., Asplund, A., Olsson, I., Edlund, K., Lundberg, E., Navani, S., Szigyarto, C. A., *et al.* (2015)

Proteomics. Tissue-based map of the human proteome. *Science* **347,** 1260419 CrossRef Medline

31. Cerami, E., Gao, J., Dogrusoz, U., Gross, B. E., Sumer, S. O., Aksoy, B. A., Jacobsen, A., Byrne, C. J., Heuer, M. L., Larsson, E., Antipin, Y., Reva, B., Goldberg, A. P., Sander, C., and Schultz, N. (2012) The cBio cancer genomics portal: an open platform for exploring multidimensional cancer genomics data. *Cancer Discov.* **2,** 401–404 CrossRef Medline
32. Gao, J., Aksoy, B. A., Dogrusoz, U., Dresdner, G., Gross, B., Sumer, S. O., Sun, Y., Jacobsen, A., Sinha, R., Larsson, E., Cerami, E., Sander, C., and Schultz, N. (2013) Integrative analysis of complex cancer genomics and clinical profiles using the cBioPortal. *Sci. Signal.* **6,** pl1 Medline
33. Robinson, D., Van Allen, E. M., Wu, Y. M., Schultz, N., Lonigro, R. J., Mosquera, J. M., Montgomery, B., Taplin, M. E., Pritchard, C. C., Attard, G., Beltran, H., Abida, W., Bradley, R. K., Vinson, J., Cao, X., *et al.* (2015) Integrative clinical genomics of advanced prostate cancer. *Cell* **162,** 454 CrossRef Medline
34. Cancer Genome Atlas Research Network. (2015) The molecular taxonomy of primary prostate cancer. *Cell* **163,** 1011–1025 CrossRef Medline
35. Grasso, C. S., Wu, Y. M., Robinson, D. R., Cao, X., Dhanasekaran, S. M., Khan, A. P., Quist, M. J., Jing, X., Lonigro, R. J., Brenner, J. C., Asangani, I. A., Ateeq, B., Chun, S. Y., Siddiqui, J., Sam, L., *et al.* (2012) The mutational landscape of lethal castration-resistant prostate cancer. *Nature* **487,** 239–243 CrossRef Medline
36. Baca, S. C., Prandi, D., Lawrence, M. S., Mosquera, J. M., Romanel, A., Drier, Y., Park, K., Kitabayashi, N., MacDonald, T. Y., Ghandi, M., Van Allen, E., Kryukov, G. V., Sboner, A., Theurillat, J. P., Soong, T. D., *et al.* (2013) Punctuated evolution of prostate cancer genomes. *Cell* **153,** 666–677 CrossRef Medline
37. Kumar, A., Coleman, I., Morrissey, C., Zhang, X., True, L. D., Gulati, R., Etzioni, R., Bolouri, H., Montgomery, B., White, T., Lucas, J. M., Brown, L. G., Dumpit, R. F., DeSarkar, N., Higano, C., *et al.* (2016) Substantial interindividual and limited intraindividual genomic diversity among tumors from men with metastatic prostate cancer. *Nat. Med.* **22,** 369–378 CrossRef Medline
38. Taylor, B. S., Schultz, N., Hieronymus, H., Gopalan, A., Xiao, Y., Carver, B. S., Arora, V. K., Kaushik, P., Cerami, E., Reva, B., Antipin, Y., Mitsiades, N., Landers, T., Dolgalev, I., Major, J. E., *et al.* (2010) Integrative genomic profiling of human prostate cancer. *Cancer Cell* **18,** 11–22 CrossRef Medline
39. Bose, R., Karthaus, W. R., Armenia, J., Abida, W., Iaquinta, P. J., Zhang, Z., Wongvipat, J., Wasmuth, E. V., Shah, N., Sullivan, P. S., Doran, M. G., Wang, P., Patruno, A., Zhao, Y., International SU2C/PCF Prostate Cancer Dream Team, *et al.* (2017) ERF mutations reveal a balance of ETS factors controlling prostate oncogenesis. *Nature* **546,** 671–675 CrossRef Medline
40. Sgouras, D. N., Athanasiou, M. A., Beal, G. J., Jr., Fisher, R. J., Blair, D. G., and Mavrothalassitis, G. J. (1995) ERF: an ETS domain protein with strong transcriptional repressor activity, can suppress ets-associated tumorigenesis and is regulated by phosphorylation during cell cycle and mitogenic stimulation. *EMBO J.* **14,** 4781–4793 CrossRef Medline
41. Stephens, D. N., Klein, R. H., Salmans, M. L., Gordon, W., Ho, H., and Andersen, B. (2013) The Ets transcription factor EHF as a regulator of cornea epithelial cell identity. *J. Biol. Chem.* **288,** 34304–34324 CrossRef Medline
42. Ando, M., Kawazu, M., Ueno, T., Koinuma, D., Ando, K., Koya, J., Kataoka, K., Yasuda, T., Yamaguchi, H., Fukumura, K., Yamato, A., Soda, M., Sai, E., Yamashita, Y., Asakage, T., *et al.* (2016) Mutational landscape and antiproliferative functions of ELF transcription factors in human cancer. *Cancer Res.* **76,** 1814–1824 CrossRef Medline
43. Sizemore, G. M., Pitarresi, J. R., Balakrishnan, S., and Ostrowski, M. C. (2017) The ETS family of oncogenic transcription factors in solid tumours. *Nat. Rev. Cancer* **17,** 337–351 CrossRef Medline
44. Goetz, T. L., Gu, T. L., Speck, N. A., and Graves, B. J. (2000) Auto-inhibition of Ets-1 is counteracted by DNA binding cooperativity with core-binding factor α2. *Mol. Cell. Biol.* **20,** 81–90 CrossRef Medline
45. Shah, N. H., Wang, Q., Yan, Q., Karandur, D., Kadlecek, T. A., Fallahee, I. R., Russ, W. P., Ranganathan, R., Weiss, A., and Kuriyan, J. (2016) An electrostatic selection mechanism controls sequential kinase signaling downstream of the T cell receptor. *Elife* **5,** e20105 CrossRef Medline
46. Shah, N. H., Löbel, M., Weiss, A., and Kuriyan, J. (2018) Fine-tuning of substrate preferences of the Src-family kinase Lck revealed through a high-throughput specificity screen. *Elife* **7,** e35190 CrossRef Medline
47. Selvaraj, N., Kedage, V., and Hollenhorst, P. C. (2015) Comparison of MAPK specificity across the ETS transcription factor family identifies a high-affinity ERK interaction required for ERG function in prostate cells. *Cell Commun. Signal.* **13,** 12 CrossRef Medline
48. Currie, S. L., Lau, D. K. W., Doane, J. J., Whitby, F. G., Okon, M., McIntosh, L. P., and Graves, B. J. (2017) Structured and disordered regions cooperatively mediate DNA-binding autoinhibition of ETS factors ETV1, ETV4 and ETV5. *Nucleic Acids Res.* **45,** 2223–2241 CrossRef Medline
49. Studier, F. W. (2005) Protein production by auto-induction in high density shaking cultures. *Protein Expr. Purif.* **41,** 207–234 CrossRef Medline
50. Currie, S. L., Doane, J. J., Evans, K. S., Bhachech, N., Madison, B. J., Lau, D. K. W., McIntosh, L. P., Skalicky, J. J., Clark, K. A., and Graves, B. J. (2017) ETV4 and AP1 transcription Factors form multivalent interactions with three sites on the MED25 activator-interacting domain. *J. Mol. Biol.* **429,** 2975–2995 CrossRef Medline
51. Ferguson, H. A., and Goodrich, J. A. (2001) Expression and purification of recombinant human c-Fos/c-Jun that is highly active in DNA binding and transcriptional activation *in vitro*. *Nucleic Acids Res.* **29,** E98 CrossRef Medline
52. Benjamini, Y., Krieger, A. M., and Yekutieli, D. (2006) Adaptive linear step-up procedures that control the false discovery rate. *Biometrika* **93,** 491–507 CrossRef
53. Hollenhorst, P. C., Shah, A. A., Hopkins, C., and Graves, B. J. (2007) Genome-wide analyses reveal properties of redundant and specific promoter occupancy within the ETS gene family. *Genes Dev.* **21,** 1882–1894 CrossRef Medline
54. Zhang, Y., Liu, T., Meyer, C. A., Eeckhoute, J., Johnson, D. S., Bernstein, B. E., Nusbaum, C., Myers, R. M., Brown, M., Li, W., and Liu, X. S. (2008) Model-based analysis of ChIP-Seq (MACS). *Genome Biol.* **9,** R137 CrossRef Medline
55. Ramírez, F., Ryan, D. P., Grüning, B., Bhardwaj, V., Kilpert, F., Richter, A. S., Heyne, S., Dündar, F., and Manke, T. (2016) deepTools2: a next generation web server for deep-sequencing data analysis. *Nucleic Acids Res.* **44,** W160–W165 CrossRef Medline
56. Machanick, P., and Bailey, T. L. (2011) MEME-ChIP: motif analysis of large DNA datasets. *Bioinformatics* **27,** 1696–1697 CrossRef Medline
57. Bailey, T. L., Boden, M., Buske, F. A., Frith, M., Grant, C. E., Clementi, L., Ren, J., Li, W. W., and Noble, W. S. (2009) MEME SUITE: Tools for motif discovery and searching. *Nucleic Acids Res.* **37,** W202–W208 CrossRef Medline
58. Thomas-Chollier, M., Sand, O., Turatsinze, J. V., Janky, R., Defrance, M., Vervisch, E., Brohée, S., and van Helden, J. (2008) RSAT: regulatory sequence analysis tools. *Nucleic Acids Res.* **36,** W119–W127 CrossRef Medline
59. Ye, J., Coulouris, G., Zaretskaya, I., Cutcutache, I., Rozen, S., and Madden, T. L. (2012) Primer-BLAST: a tool to design target-specific primers for polymerase chain reaction. *BMC Bioinformatics* **13,** 134 CrossRef Medline